On the Performance of Small-Sized Venturi Flowmeters in Cavitating and Non-Cavitating Flow Regimes

Max Kandula[1], Brian M. Nufer[2]
NASA Kennedy Space Center, Florida 32899

The performance of venturi in the cavitating and non-cavitating flow regimes has been discussed theoretically and experimentally. Pressure drop test data with water was obtained with a 0.0355 inch throat venturi with pressure drop measured between the inlet and the outlet of the venturi, typical of practical venturi measurements on spacecraft. The pressure drop data acquired in the non-cavitating regime at relatively low flow rates display low Reynolds number effects on the discharge coefficient. A theoretical discussion of the corresponding discharge coefficients in the two flow regimes along with comparisons with test data are presented. For non-cavitating flow regime of unique venturi geometries of relatively small throat size, test data required low Reynolds number correction factor for the discharge coefficient in terms of throat Reynolds number. The application of existing theory is not straightforward for the unique geometries under consideration.

Nomenclature

D	=	tube internal diameter
d	=	venturi throat diameter
$\dot{m}$	=	mass flow rate
p	=	pressure
T	=	temperature
V	=	velocity
β	=	d / D
μ	=	dynamic viscosity of fluid
ρ	=	density of fluid

Subscripts

t	=	throat
1	=	pressure tap at inlet (upstream of throat)
2	=	pressure tap at outlet (downstream of throat)

I. Introduction

Venturi flowmeters are considered frequently in flight propulsion systems and many other industrial applications. The performance of the venturi meter both in the non-cavitating and cavitating regimes has been extensively investigated. The pressure drop across the venturi is presented in terms of discharge coefficient treated as a function of Reynolds number. The discharge coefficient represents the ratio of the actual mass flow rate to the theoretical flow rates and accounts for the influence of flow contractions, expansions, and frictional effects.

A schematic configuration of the venturi is displayed in **Fig**. 1 (as adapted from Scroggins[1]), showing the locations of venturi inlet, throat, and outlet sections, denoted by 1, t and 2 respectively. The flow direction is from left to right, as indicated.

[1] Technical Fellow, KBR, Mail Stop LASSO-001, Associate Fellow, AIAA
[2] OSAM-1 Propellant Transfer Assembly Lead, Exploration Payloads Branch, Mail-Stop NE-L5

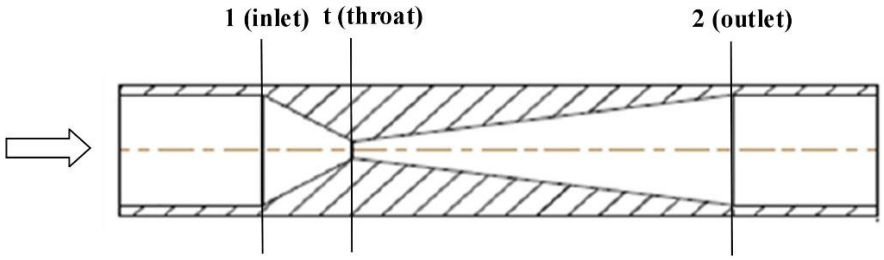

Fig. 1 Schematic of a flow venturi (adapted from Scroggins[1])

Ideally, the downstream pressure tap for the venturi is located at the venturi throat (or neck) to facilitate a large (significant) pressure drop. The location of the downstream pressure presents no difficulty if the throat diameters are relatively large. In flight propulsion system applications, typical venturi throat diameters are relatively small, which makes it difficult to install a pressure tap at the throat without disturbing the flow appreciably. For this reason, the downstream pressure tap is located far from the throat (near the outlet) where the flow cross-sectional area is essentially the same as that of the inlet.

There is relatively scant discussion in the literature on the discharge coefficients of venturi with a downstream pressure tap located relatively far downstream of the throat. The purpose of this article is to present experimental data and theoretical analysis concerning the discharge coefficient of a venturi under such circumstances both in the cavitating and non-cavitating regimes.

II. Analysis of Venturi Performance: Theoretical Considerations

A. Performance of Cavitating Venturi

1. *Cavitation Regime (Inception)*

A practical measure of cavitation initiation in venturis is expressed by the so-called cavitation number σ defined variously. One common form of cavitation number is defined by (Martin et al.[2]):

$$\sigma = \frac{p_2 - p_{\text{sat}}}{\frac{1}{2}\rho V_{\text{t}}^2} \tag{1}$$

where p_2 is the pressure downstream (outlet) of the venturi, p_{sat} is the saturation pressure corresponding to the temperature of the fluid, V_t is the throat velocity, and ρ is the liquid density. Eq. (1) shows that cavitation occurrence is possible when the cavitation number is unity.

As the saturation pressure and the throat pressure are relatively small in comparison with the upstream pressure for the conditions studied, it can be shown that the cavitation number is satisfactorily approximated by the relation (Niedzwiedzka and Sobieski[3]):

$$\sigma \simeq p_2 / p_1 \tag{2}$$

Figure 2 shows the experimental mass flow rate ratio (mass flow rate to critical or maximum mass flow rate) as a function of pressure ratio p_2 / p_1 across the venturi. For pressure ratios smaller than 0.8, cavitation occurs, and the flow becomes choked. When the pressure ratio exceeds 0.8, cavitation does not occur. Existing test data confirm this

trend. In general, the critical pressure ratio depends strongly on the geometric parameters of the venturi, such as throat area ratio and diffuser angle of the venturi (Ebrahimi et al.[4]). Data by Ashrafizadeh et al.[5] show that keeping other parameters unchanged, the critical pressure ratio decreases form 0.72 to 0.6 as the diffuser angle increases from 5^0 to 15^0.

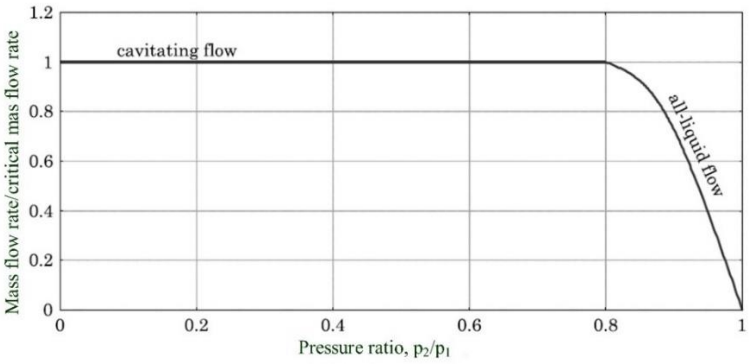

Fig. 2 Characteristic curve for a cavitating venturi (Niedzwiedzka et al[3]).

The preceding plot describes the onset of cavitation for low subcooling, small pressure loss, and very small sizes. In the presence of large superheats at the throat (such as occur in cryogenic systems), the mass flow will exceed the choked flow (see **Fig.** 3a taken from Chen and Navickas[6]). Starting at point B and decreasing the pressure ratio point C may be reached before nucleation begins. At this point the flow will drop from point C to point D. **Fig**. 3b shows typical experimental data for a cavitating venturi with ammonia flow. The downstream pressure is adjusted by supplying heater power. The venturi chokes at a pressure ratio 0.25. Transient conditions were shown to prevail under certain conditions.

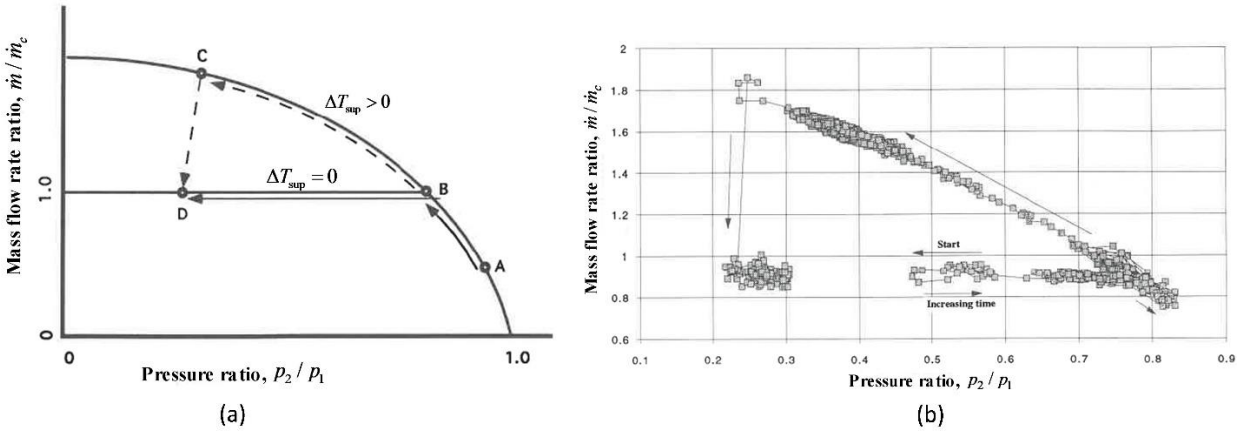

Fig. 3 Characteristic curves for cavitating venturi for low and large superheats (Chen and Navickas[4]).

2. *Mass Flow Rate*

For a venturi operating the cavitation region, the mass flow rate becomes independent of downstream (outlet) pressure, and depends only on the inlet pressure as expressed by:

$$\dot{m} = C_{dc} \frac{A_t \rho}{\sqrt{1-\left(A_t / A_1\right)^2}} \sqrt{\frac{2p_1}{\rho}} \sim C_{dc} A_t \rho \sqrt{\frac{2p_1}{\rho}} \tag{3a}$$

where the coefficient of discharge C_{dc} for the is a function of throat Reynolds number Re_t **:**

$$C_{dc} = C_{dc}\left(\mathrm{Re}_t\right) \tag{3b}$$

and the throat Reynolds number is defined by

$$\mathrm{Re}_d = \rho V_t d / \mu \tag{3c}$$

B. Pressure Recovery in a Venturi

Figure 4 displays the characteristic pressure distribution in a venturi (Suesser[6]). In the converging section, the static pressure decreases along the axis while the dynamic pressure increases. The opposite is true in the diverging section. The pressure level at the throat goes to a minimum, with subsequent recovery downstream of the throat. The permanent pressure drop (loss) of venturi tubes (measured at the downstream tap) is relatively low compared with that for all other differential-producing devices (orifice, etc.). For example, for $\beta = 0.66$ and throat Reynolds number of 100,000, the calculated discharge coefficients of a venturi and an orifice are 0.97 and 0.62 respectively (Hollingshead et al.[7]). This shows that for a given area ratio and throat Reynolds number, at the same mass flow rate, the (permanent) pressure drop through a venturi is much less than that of the venturi. Note that the absolute value of the venturi outlet (downstream pressure) or the back pressure is a function of the fluid system resistance downstream. The venturi geometric design (convergence and divergence angles, throat area ratio) for a given range of mass flow rates and pressure drop is dictated by the system requirements.

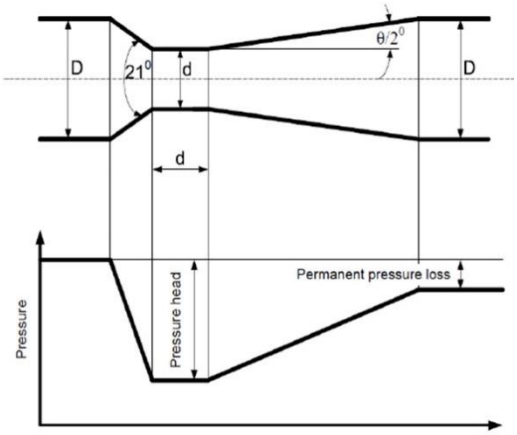

Fig. 4 Schematic of pressure recovery in a venturi (Suesser[4]).

Figure 5 presents the data of Suesser[8] for discharge coefficient for the cavitating region (Figure 5a) and the permanent pressure loss for the non-cavitating region (Figure 5b). In the cavitation region, the discharge coefficient increases slightly with the throat Reynolds number. In the non-cavitating region, the permanent pressure drops as a fraction of the pressure head at the throat decreases with an increase in throat Reynolds number. It would be more convenient to recast the y-axis in Figure 5b in terms of a discharge correction factor as a function of throat Reynolds number. This is carried out in the present work.

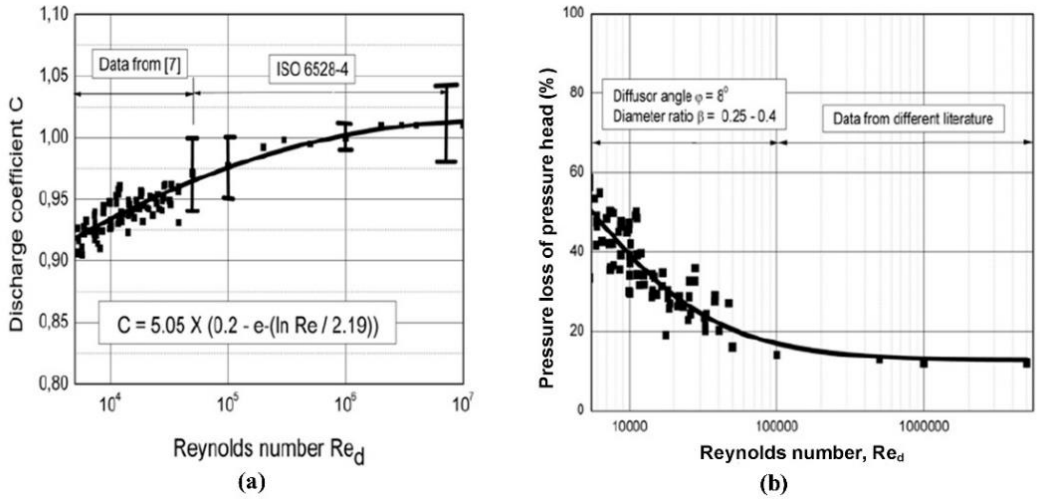

Fig. 5 Venturi performance data from Suesser[4] for (a) cavitating region and (b) non-cavitating region.

C. Performance of Non-Cavitating Venturi

1. *Venturi Performance Based on Throat Pressure*

The mass flow rate through a *non-cavitating (non-choked) venturi* is traditionally determined from the well-known relation:

$$\dot{m} = C_{dn} \frac{A_t \rho}{\sqrt{1-\left(A_t / A_1\right)^2}} \sqrt{\frac{2\Delta p_t}{\rho}} \tag{4a}$$

where C_{dn} is the coefficient of discharge for the *non-cavitating venturi*, A_t is the throat cross-sectional area, A_1 is the inlet cross-sectional area, ρ is the fluid density, and Δp_t is the pressure drop (*inlet to throat*) defined by:

$$\Delta p_t = p_1 - p_t \tag{4b}$$

The quantities p_1 and p_t refer to the static pressure at the inlet and the throat respectively.

Since the throat pressure is not measured (due to difficulty of measurement) in the test as is usually the case with small-sized venturis (with small diameter throat), it can be evaluated from the inlet pressure p_1 or the exit pressure (or back pressure) p_2 with the aid of Bernoulli equation. For example, the throat pressure is evaluated from the (frictionless) Bernoulli equation and the inlet pressure:

$$p_1 + \frac{1}{2} V_1^2 = p_t + \frac{1}{2} \rho V_t^2 \tag{5a}$$

or

$$p_2 + \frac{1}{2} V_2^2 = p_t + \frac{1}{2} \rho V_t^2 \tag{5b}$$

where V_t is the throat velocity, d is the throat diameter, and μ is the dynamic viscosity of the test liquid. The sum of the two terms on each side of (5a) refers to the total pressure, which is the sum of the static pressure and the dynamic pressure (velocity head). The throat velocity is determined from the mass flow rate $\dot{m}$ as:

$$V_t = \dot{m} / \left(\rho A_t \right) \tag{5c}$$

The coefficient of discharge for the venturi C_{dn} is generally correlated with the *throat Reynolds number* Re_t :

$$C_{dn} = C_{dn} \left(\mathrm{Re}_d \right) \tag{6}$$

where the throat Reynolds number is defined by Eq. (3c).

2. *Venturi Performance Based on Pressure Downstream of Throat*

In practical applications involving relatively small-sized non-cavitating venturis, the measurement of throat pressure is difficult, and the venturi performance is conveniently based on the measurement of venturi outlet pressure sufficiently downstream of the throat (where $A_1 = A_2$, and therefore $V_1 = V_2$), where it is easy to measure the static pressure rather than at the throat. Under these conditions, the mass flow rate of water can be determined from (Ghassemi and Fasih[9]):

$$p_1 + \frac{1}{2} \rho V_1^2 = p_2 + \frac{1}{2} \rho V_2^2 + K_2 \frac{1}{2} \rho V_2^2 \tag{7}$$

where K_2 is an overall (effective) pressure loss coefficient through the venturi. Since $V_1 = V_2$, this equation reduces to

$$p_1 - p_2 = \Delta p_{12} = K_2 \frac{1}{2} \rho V_2^2 \tag{8}$$

Using the relation

$$\dot{m} = \rho V_2 A_2 \tag{9}$$

we find that

$$K_2 = \frac{A_2^2 \sqrt{2 \rho \Delta p}}{\dot{m}^2} \tag{10}$$

The factor K_2 accounts for pressure drop through the entrance of venturi (sudden contraction), convergent portion (gradual contraction), divergent portion (gradual expansion) and exit of venturi (sudden expansion) and friction losses. Under these conditions, the mass flow rate through the venturi is expressed by:

$$\dot{m} = A_2 \sqrt{\frac{2 \rho \left(p_1 - p_2 \right)}{K_2}} \tag{11}$$

where A_2 is the outlet cross sectional area of the venturi. The loss coefficient K_2 depends on the geometry of the venturi and on the flow Reynolds number.

For scaling purposes, Eq. (8) can be alternatively expressed as:

$$\dot{m} = K A_t \sqrt{2 \rho \left(p_1 - p_2 \right)} \tag{12a}$$

where

$$K = \frac{A_2}{A_t} \sqrt{\frac{1}{K_2}} \tag{12b}$$

is an overall discharge coefficient for the non-cavitating region based on pressure drop at the downstream tap. In order to take into account the Reynolds number effect on the mass flow rate, it is convenient to express the coefficient K as

$$K = K_0 \phi \left(\mathrm{Re}_d \right) \tag{13}$$

where K_0 is the coefficient of discharge at high Reynolds number, and $\phi(\mathrm{Re}_d)$ is a dimensionless coefficient accounting for Reynolds number effects (action of viscosity) on the overall discharge coefficient.

III. Venturi Configuration

Figure 6 shows the configuration of the 0.0355 inch throat venturi (d) tested at KSC. The overall length of the venturi is 1.5 inch, whereas the total length of the convergent and divergent portions of the venturi is 0.75 inch (the remainder being straight tubes at the inlet and the outlet). The outer diameter of the inlet and the outlet is 0.250 inches and the inner diameter D is 0.210 inches. The throat area ratio $\beta = d / D = 0.17$. The semi-angle of divergence is 10 deg. Test data were obtained at a water temperature of 17 deg C (63 deg F).

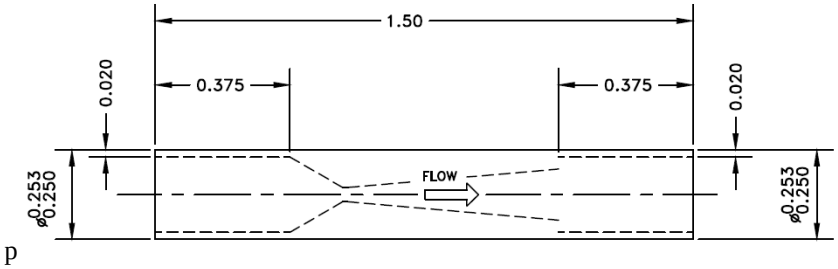

p

Fig. 6 Schematic of venturi configuration.

IV. Test Setup for Venturi Testing

A simplified test setup was considered for investigating performance of the cavitating venturi (**Fig**. 7a). A high-accuracy Coriolis flow meter (FM-04) served as the standard for characterizing the cavitating venturi. The pressure gauge PGT-07 (0-600 psig) is placed upstream of the venturi, and the pressure gauge PGT-08 (0-600 psig) is placed downstream of the throat (at about 2.75 inches downstream of the throat), where the local cross-sectional area of the tube is the same as that of the venturi inlet. A wider range of mass flow rates were obtained with the aid of a needle valve. From the measured flow rate and the pressure drop across the venturi, the venturi performance is characterized. Separate tests were performed to investigate the venturi performance in the non-cavitating and the cavitating regimes.

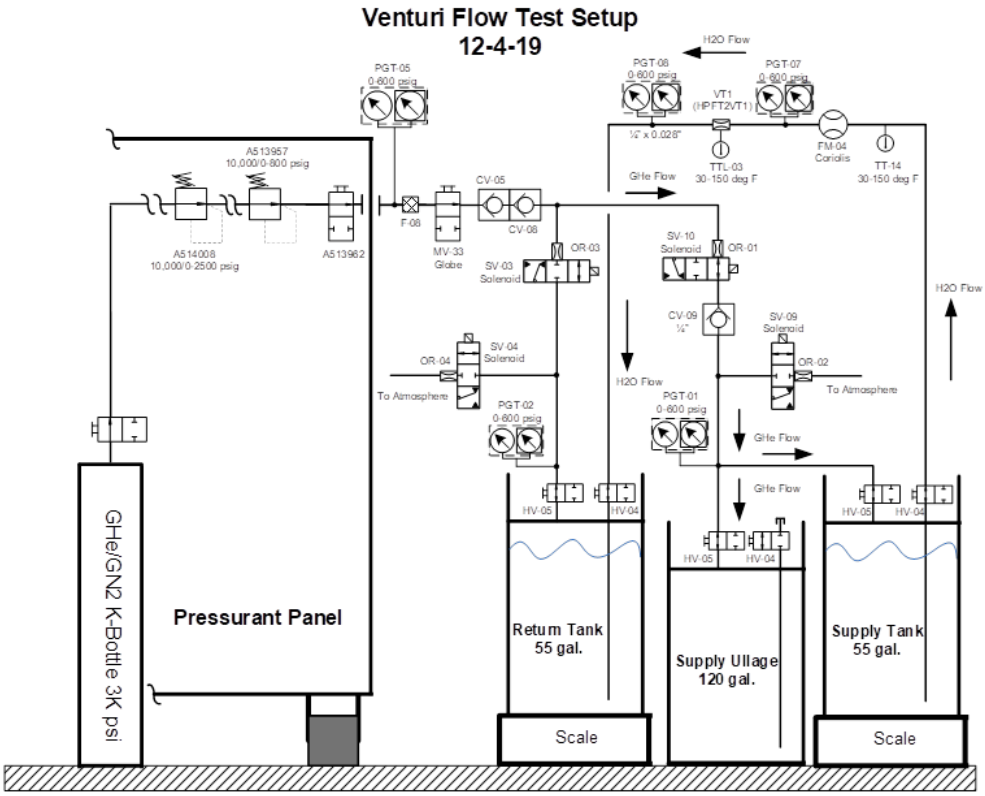

Fig. 7a Schematic of venturi test setup.

Figure 7b displays a photograph of the venturi test section along with the pressure gauges. This image is useful as a reference to show the relative dimensions of the test measurements.

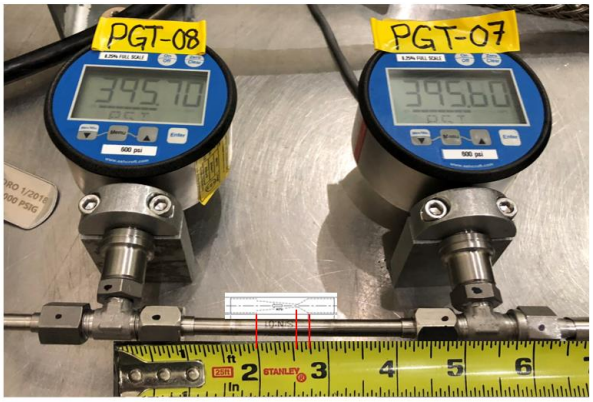

Fig. 7b Photograph of the venturi test section.

The test duration was about 58 min. In the test, the inlet pressure was held constant, while the pressure ratio (venturi outlet to inlet pressure) was varied. This preliminary test data contained the cavitation region in addition to the non-cavitating region. The mass flow rate was varied from 0.2 to 5.0 lbm/min. The mass flow rate, pressure, and temperature measurement uncertainties are respectively about +/-0.5%, +/-1.5 psia and +/-1.8 deg F.

V. Results

A. Results and Comparisons for the Non-Cavitating Region

The mass flow rate in the non-cavitating region is correlated as:

$$\dot{m} = K_0 \phi(\mathrm{Re}_d)\sqrt{2\rho(p_1 - p_2)} \tag{13a}$$

where

$$\frac{A_2}{A_t\sqrt{K'}}, \quad \mathrm{Re}_d = \frac{\rho V d}{\mu} \tag{13b}$$

Comparison of Eq. (13) with the KSC data (for which $A_2 / A_t = 39.2$) suggest a value of $K_0 = 2$, which may be considered for pressure drop estimations in the non-cavitating mode.

Figure 5 compares the non-cavitating correlation equation (1) with the low flow venturi KSC test data. Excellent agreement is noted between the theory and the data for flow rates down to 1.5 lbm/min. For flow rates in excess of 1.5 lbm/min, both the theory and the data show a linear variation of the flow rate with the square root of the pressure drop. However, for flow rates below 1.6 lbm/min, the data exhibits a transition to a parabolic form (with the data extending down to 0.2 lbm/min). This parabolic dependence, when extrapolated, suggests a proper limit at the zero flow rate, where the pressure drop approaches zero (as we would expect). The data suggest that in this very small flow rate range, for a given flow rate, the pressure drop exceeds that given by the linear theory. This shows that low-Reynolds number viscous effects become predominant at very low flow rates, requiring low-Reynolds number corrections to the correlation (which appear as a correction to the discharge coefficient). For example, see Kandula et al. (2019) for low Reynolds-number effects discussed with respect to orifice flow of gases.

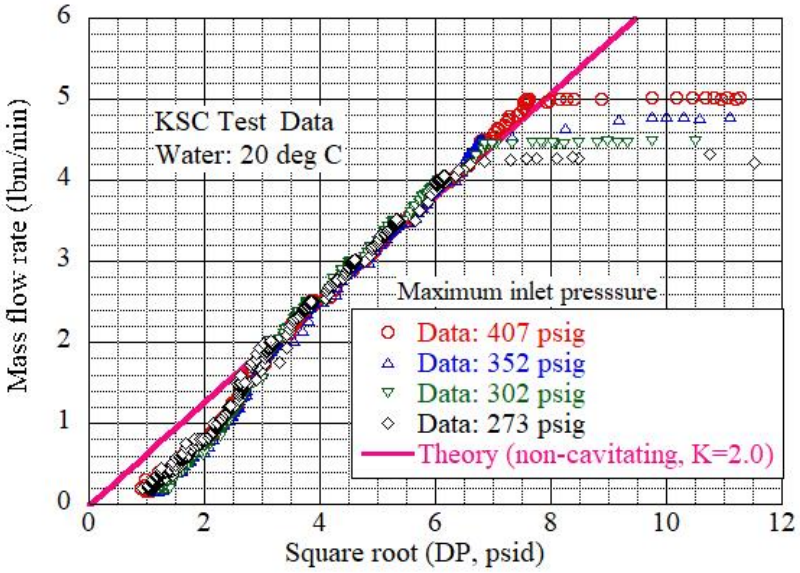

Fig. 5 Mass flow rate as a function of the pressure drop in the low flow rate regime.

Figure 8 displays the discharge correction factor ϕ for the venturi as a function of throat Reynolds number, as deduced from a comparison of the measurements and the theory in the non-cavitating mode. The lowest throat Reynolds number in the data is found to be about 20,000, at which the Reynolds number correction factor reduces to 0.15. These present results are compared with the data Suesser4. The discharge correction factors for the data OF Suesser[4] were deduced from the data presented in the form of permanent pressure loss (as a percent of pressure head at the throat). The present data show the Reynolds number effects become significant below throat Reynolds number

of about 20,000, whereas in the data of Suesser[4] Reynolds number effects persist up to throat Reynolds number of a million. The semi-angle of divergence is 8 deg in these tests, as opposed to 10 deg in the present tests. The differences in the discharge correction factors are attributable primarily to the difference in the divergence angle of the venturi.

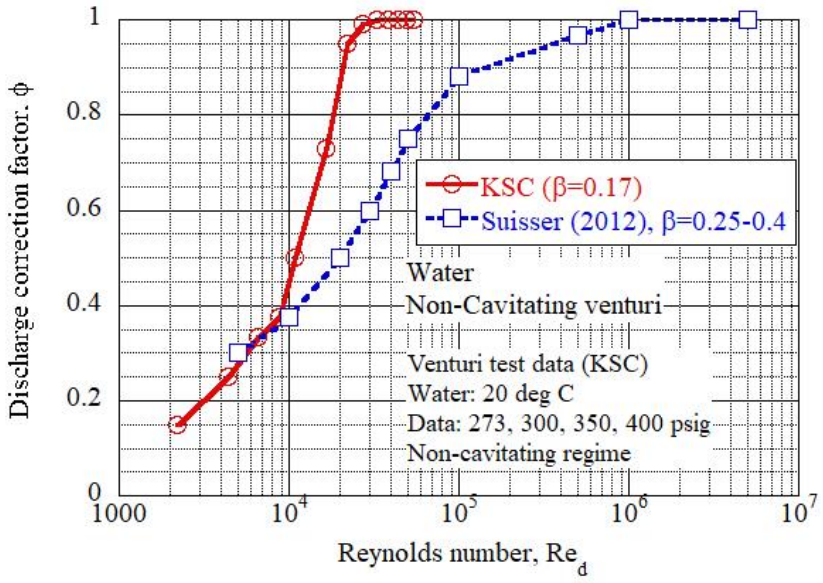

Fig. 8 Drag correction factor for the venturi as a function of throat Reynolds number in the non-cavitating region.

B. Results and Comparisons for the Cavitating Region

For the cavitation tests, the inlet pressure is varied from 412 psia to 64 psia, while the outlet pressure is held at nearly 22 psia. **Fig**. 9 illustrates a comparison of the critical mass flow rate as a function of the square root of the inlet pressure from the test data. For the cavitation regime, the data covers a wider range of mass flow rates from 2.1 to 5.3 lbm/min.

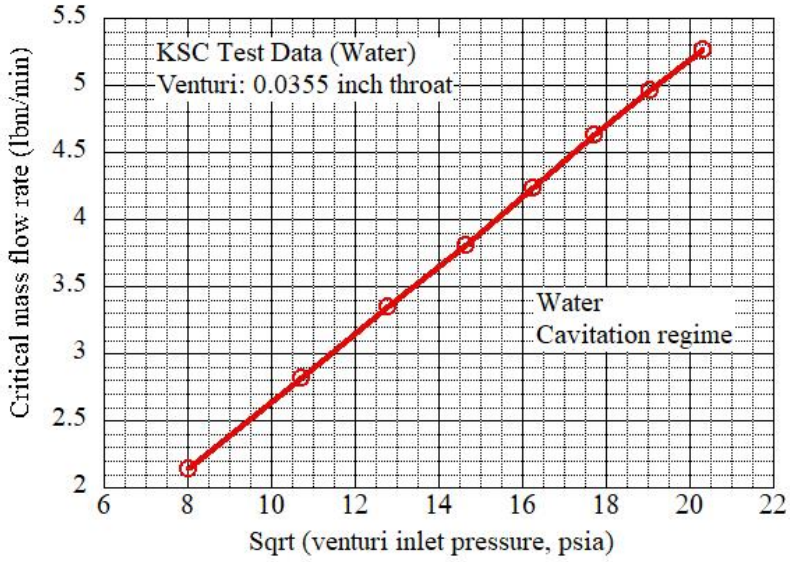

Fig. 9 Mass flow rate as a function of the inlet pressure from KSC data in the cavitation region.

For a venturi operating in the cavitation regime, the mass flow rate becomes independent of downstream (outlet) pressure, and depends only on the inlet pressure as expressed by (12a). **Fig.** 10 displays a comparison of the coefficient of discharge C_d in the cavitation mode from KSC data as a function of venturi throat Reynolds number. Data set 1 were obtained from tests data shown in Fig. 9, while data set 2 correspond to the data shown in Fig. 5 for the cavitation region. The KSC data show an average of about 0.84 (varying from 0.83 to 0.86), with a trend of decreasing discharge coefficient with an increase in the throat Reynolds number, approaching a constant value. This is contrary to the trend seen in Fig. 5a (data of Suesser[3]).

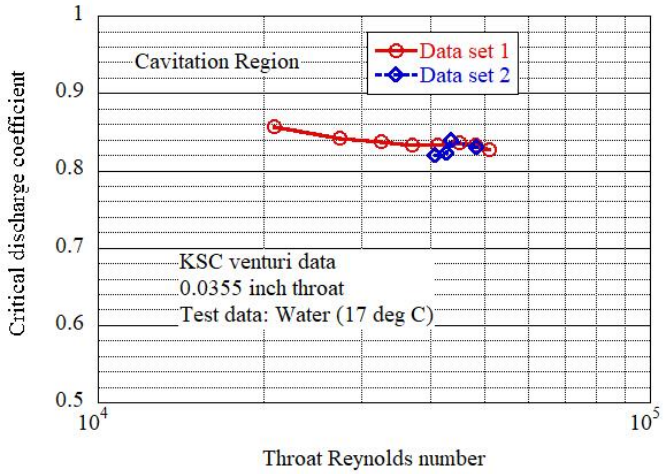

Fig. 10 Comparison of the discharge coefficients in the cavitation region.

VI. Conclusions

Water test data for flow rates and pressure drop through the venturis have been obtained both in the non-cavitating and cavitating regions. For the non-cavitating mode, correlation for mass flow rate through the venturi as a function of pressure drop has been developed based on existing test data for water. A correction factor for the discharge coefficient in terms of throat Reynolds number has been presented. For cavitating flow, the critical mass flow rate through the venturi depends on the supply pressure, and a discharge coefficient is correlated in terms of the throat Reynolds number.

Acknowledgments

This work was funded by the NASA's Exploration and In-Space Services (NExIS) Division, Goddard Space Flight Center in cooperation with NASA Kennedy Space Center.

References

[1]Scroggins, A., A streamlined approach to venture sizing, AIAA-2012-4028, 48th AIAA/ASME/SAE/ASEE Joint Propulsion Conference, Atlanta, Ga, 2012.

[2]Martin, C.S., Medlarz, H., Wiggert, D.C., and Brennan, C., Cavitation inception in spool valves, J. Fluids Engineering, Vol. 103, pp. 564-575, 1981.

[3]Niedzwiedzka, A., and Sobieski, W., Analytical analysis of cavitating flow in venturi tube on the basis of experimental data, Technical Sciences, Vol. 19, No. 3, pp. 215-229, 2016.

[4]Ebrahimi, B., et al., Characterization of high-pressure cavitating flow through a cavitating flow through a thick orifice plate through a pipe of constant cross-section, International Journal of Thermal Sciences, Vol. 114, pp. 229-240, 2017.

[5]Ashrafizadeh, A.M., and Ghassemi, H., Experimental and numerical investigation on the performance of small-sized cavitating venturis, Flow Measurements and Instrumentation, Vol. 42, pp. 6-15, 2015.

[6]Chen, L.L., and Navickas, J., The behavior of small cavitating venturis in low subcooling and pressure loss range, Advances in Cryogenic Engineering, Vol. 39, pp. 1059-1064, ed. P. Kittel, Plenum Press, New York, 1994.

[7]Suesser, M., Performance of classical venturi tubes for application in cryogenic facilities, AIP Conference Proceedings, 1434, 1636, 2012.

[8]Hollingfhead, C.L., Johnson, M.C., Barfuss, S.L., and Spall, R.E., Discharge coefficient of venturi, standard concentric orifice plates, V-cone and wedge flow meters at low Reynolds numbers, Journal of Petroleum Science and Engineering, Vol. 78, pp. 559-566, 2011.

[9]Ghassemi, H., and Fasih, H.F., Application of small size cavitating venturi as flow controller and flow meter, Flow Measurement and Instrumentation, Vol. 22, pp. 406-412, 2011.